

Empirical Removal of Artifacts from the ISCCP and PATMOS-x Satellite Cloud Records

JOEL R. NORRIS AND AMATO T. EVAN

Scripps Institution of Oceanography, La Jolla, California

(Manuscript received 11 March 2014, in final form 8 November 2014)

ABSTRACT


The International Satellite Cloud Climatology Project (ISCCP) dataset and the Pathfinder Atmospheres–Extended (PATMOS-x) dataset are two commonly used multidecadal satellite cloud records. Because they are constructed from weather satellite measurements lacking long-term stability, ISCCP and PATMOS-x suffer from artifacts that inhibit their use for investigating cloud changes over recent decades. The present study describes and applies a post hoc method to empirically remove spurious variability from anomalies in total cloud fraction at each grid box. Spurious variability removed includes that associated with systematic changes in satellite zenith angle, drifts in satellite equatorial crossing time, and unrealistic large-scale spatially coherent anomalies associated with known and unidentified problems in instrument calibration and ancillary data. The basic method is to calculate for each grid box the least squares best-fit line between cloud anomalies and artifact factor anomalies, and to let the residuals from the best-fit line be the newly corrected data. After the correction procedure, the patterns of regional trends in ISCCP and PATMOS-x total cloud fraction appear much more natural. The corrected data cannot be used for studies of globally averaged cloud change, however, because the methods employed remove any real cloud variability occurring on global scales together with spurious variability. An examination of Moderate Resolution Imaging Spectroradiometer (MODIS) total cloud fraction data indicates that removing global-scale variability has little impact on regional patterns of cloud change. Corrected ISCCP and PATMOS-x data are available from the Research Data Archive at NCAR.

1. Introduction

Clouds have a large impact on the earth's radiation budget. They typically reflect more solar radiation back to space than the unobscured surface and emit less thermal infrared radiation to space than the clear-sky atmosphere. Optically thick low-level clouds have a net cooling effect on the climate system because they reflect much solar radiation and emit much thermal radiation due to their relatively warm temperature. Optically thin high-level clouds have a net warming effect on the climate system because they reflect little solar radiation and emit little thermal radiation due to their relatively cold temperature. In the current global average, the loss

of energy through solar reflection by clouds exceeds the gain of energy through greenhouse warming by clouds (Ramanathan et al. 1989). Change in the horizontal extent, optical thickness, height, and other properties of clouds in response to global warming will modify reflection of solar radiation and emission of thermal radiation and may exert a feedback on the climate system. How cloud properties will change is poorly known, however, and remains a key uncertainty in our understanding of climate change (Stocker et al. 2013; Dufresne and Bony 2008).

One reason for this uncertainty is a lack of a simple fundamental theory for how climate change will affect a large variety of cloud types with differing radiative impacts. Another reason is that global climate models have difficulty properly representing subgrid-scale cloud processes and produce cloud simulations that are inconsistent with one another and with observations (e.g., Clement et al. 2009; Klein et al. 2013). The shortcomings of theory and global climate models motivate the alternative approach of observing how clouds have changed in recent decades, a time period of rapidly increasing anthropogenic forcing and warming of the climate system. If

 Denotes Open Access content.

Corresponding author address: Joel Norris, Scripps Institution of Oceanography, University of California, San Diego, 9500 Gilman Drive, Dept. 0206, La Jolla, CA 92093-0206.
E-mail: jnorris@ucsd.edu

DOI: 10.1175/JTECH-D-14-00058.1

patterns of multidecadal cloud variability likely to be associated with anthropogenically forced climate change were to be identified in the observational record, this would help constrain global climate model simulations and reduce cloud feedback uncertainty. Unfortunately, currently available cloud records are not sufficiently reliable to detect real cloud changes over decades over much of the earth.

Observational systems designed for monitoring weather are the only source of cloud records spanning multiple decades. These lack long-term stability needed for monitoring climate; new instruments, calibration drifts, orbital changes, and other factors have introduced spurious variability that usually overwhelms any real long-term signal in surface and satellite cloud records (e.g., Norris 1999, 2000; Campbell 2004; Evan et al. 2007; Norris and Slingo 2009; Foster and Heidinger 2013; Free and Sun 2013). Although the presence of large systematic artifacts currently prevents the use of satellite cloud data in studies of long-term cloud variability, the fact that the artifacts are systematic provides the opportunity to characterize and empirically remove them. If similar cloud variability is found in multiple independent satellite datasets after removal of artifacts, then it will increase our confidence that the reported cloud changes are real.

The present study characterizes and empirically removes spurious variability from the two most widely used lengthy satellite cloud records: the International Satellite Cloud Climatology Project (ISCCP) and the Pathfinder Atmospheres–Extended (PATMOS-x) dataset (Rossow and Schiffer 1999; Heidinger et al. 2014). One type of artifact is a systematic relationship between changes in reported cloud fraction and changes in geostationary satellite zenith angle that is present in ISCCP (Campbell 2004; Evan et al. 2007). Another type of artifact is a systematic relationship between changes in reported cloud fraction and changes in equatorial crossing time that predominantly affects PATMOS-x (Jacobowitz et al. 2003; Foster and Heidinger 2013; Heidinger et al. 2014). A third type of artifact is related to transitions between satellites and effective changes in calibration that produce spatially coherent changes in cloud fraction at every location viewed by a satellite. This artifact is present in both ISCCP and PATMOS-x (Norris 2000; Norris and Slingo 2009).

Although the essential reasons for many satellite cloud artifacts can be identified, we have insufficient information and understanding of the physics to reprocess the data on the basis of first principles. Instead, we apply a post hoc correction. The fact that presumably spurious anomalies in ISCCP cloud fraction systematically vary with anomalies in satellite zenith angle

enables us to empirically characterize that relationship via linear regression. Residual anomalies from the best-fit line correspond to cloud variability that is mostly free of spurious effects from changing zenith angle. We remove effects of other types of artifacts in a similar manner. The result is corrected versions of the ISCCP and PATMOS-x satellite cloud datasets in which natural rather than spurious variability predominates on multiyear and longer time scales. Although not suitable for monitoring variability in global mean cloudiness, the corrected cloud datasets will enable investigation of changes in regional cloud patterns, relative to an unknown global mean change, during the past several decades.

2. Data and methods

a. ISCCP

The ISCCP (Rossow et al. 1996; Rossow and Schiffer 1999) provides information on cloud properties obtained from weather satellite measurements starting July 1983 and currently ending in December 2009. Geostationary satellites are the primary source of measurements in ISCCP equatorward of 55° latitude, but polar-orbiting satellites are used when and where geostationary satellites are not available. Retrievals of cloud fraction, cloud optical thickness, cloud-top pressure, and other cloud properties are accomplished using visible (VIS), window-IR, and near-IR radiances in combination with ancillary data inputs. In addition to total cloud fraction, ISCCP provides cloud fraction within seven intervals of cloud-top pressure and six intervals of cloud optical thickness (i.e., cloud fraction for each of 42 “types”). Cloudy pixels are identified if they are brighter in the visible channel or colder in the thermal infrared channel than presumed clear-sky pixels, beyond certain thresholds.

Our starting cloud record is ISCCP D1 3-hourly cloud data in ~280-km equal-area grid boxes. All calculations are performed on the equal-area grid and then linearly interpolated in longitude to a 2.5° × 2.5° equal-angle grid. We use only daytime observations (defined as solar zenith angle < 78°) because visible radiances aid the detection of clouds. This has very little impact on long-term variability because monthly anomalies in total cloud fraction retrieved from day and night IR radiances are very similar to monthly anomalies in total cloud fraction retrieved from daytime VIS+IR radiances. We exclude cloud data poleward of 60° latitude from our correction procedures because passive retrieval of cloud properties is difficult over bright and cold surfaces, and no visible retrievals can be made during polar night. Monthly anomalies are calculated by subtracting the long-term mean for each calendar month from the cloud

fraction values at each grid box. For ISCCP, we often use 3-hourly anomalies, which are calculated by subtracting the long-term mean for each calendar month and UTC hour.

b. PATMOS-x

The PATMOS-x dataset (Heidinger et al. 2014) provides information on cloud properties obtained from weather satellite measurements starting in October 1981. We use data starting in July 1983 and ending in December 2009 for consistency with ISCCP. All PATMOS-x products are retrieved via radiances measured by the five-channel Advanced Very High Resolution Radiometers (AVHRR) on polar-orbiting satellites (here, AVHRR refers only to the five-channel imager and not the four-channel instruments flown on the TIROS-N and NOAA-8 and NOAA-10 satellites). The AVHRR instruments measure radiances for two visible, two window infrared, and one near-infrared channels. Cloud fraction is determined using a naïve Bayesian classifier trained using collocated measurements from an AVHRR and the Cloud–Aerosol Lidar with Orthogonal Polarization instrument (Heidinger et al. 2012). The predictors for cloud fraction include metrics of spatial homogeneity in the thermal channels, retrieved versus forward modeled clear-sky emissivity, visible reflectance, and the split-window infrared difference.

Our starting cloud record is PATMOS-x, version 5, level 3 “GEWEX” data, which provides retrievals of cloud fraction, type, height, and other products globally in $1^\circ \times 1^\circ$ equal-angle grid boxes. We converted these to $2.5^\circ \times 2.5^\circ$ equal-angle grid boxes for consistency with ISCCP. During the first decade and a half of the PATMOS-x record, measurements were made by a single AVHRR instrument flying on one satellite in an “afternoon orbit” (i.e., crossing the equator at 0130 and 1330 local time). Outside of polar regions, this satellite provided one nighttime and one daytime observation of every point on Earth. A “morning” satellite (1030 local equatorial crossing time) was subsequently added in 1992, and there were at least two satellites with AVHRR instruments collecting data at any one time during the latter part of the record (two nighttime and two daytime observations). For consistency over the entire PATMOS-x record and with ISCCP, our analysis employs products only from the ascending (daytime) orbit of “afternoon” satellites. We exclude retrievals with a solar zenith angle greater than 88° , since those do not use visible channels. We also exclude all data during the months of January 1985, December 1988, and from October 1994 through June 1995 due to poor-quality retrievals arising from sensor degradation at the end of the satellite lifetime. We obtained solar and satellite geometry data directly from

the PATMOS-x website via the PATMOS-x level 3 archive, but at the time of writing these data were in the process of being made available from the National Climatic Data Center.

c. MODIS

The Moderate Resolution Imaging Spectroradiometer (MODIS) instrument provides information on cloud properties starting in March 2000 for the morning *Terra* satellite and July 2002 for the afternoon *Aqua* satellite. The present study uses *Aqua* data to better match the afternoon satellites contributing to PATMOS-x. Although the record is too short for investigation of multi-decadal cloud variability, it is a useful comparison to ISCCP and PATMOS-x. Unlike ISCCP and PATMOS-x, *Aqua* MODIS is a single instrument with much more stable calibration on a satellite strictly maintaining a sun-synchronous orbit. Consequently, *Aqua* MODIS cloud data do not exhibit large artifacts due to calibration or orbital drift. We use daytime-only MODIS cloud fraction on a $1^\circ \times 1^\circ$ equal-angle grid from the MYD08 Collection 6 product (Baum et al. 2012).

d. General method for removing artifacts

Cloud fraction retrieved by a satellite depends on many variables. Meteorological conditions control cloudiness, but the reported cloud fraction may be affected by additional conditions related to the observing system, such as satellite zenith angle. We can express retrieved cloud fraction as a function of various factors as follows:

$$C = C(a_1, a_2, \dots, r_1, r_2, \dots), \quad (1)$$

where C is cloud fraction, a_i are factors producing artificial variability, and r_i are factors producing real variability. Classifying some factors as artificial does not entail that no real physical effects are involved but rather that they lead to a systematic bias in retrieved cloud fraction. Note that C , a_i , and r_i vary with time and location.

Our goal is to remove the effects of variability in artifact factors a_i from variability in cloud fraction C . Since we do not know the functional dependence of C on a_i from first principles, we must do so on a post hoc basis. We begin by expressing Eq. (1) as a first-order Taylor series expansion about the climatological mean at each grid box,

$$\begin{aligned} C(a_1, a_2, \dots, r_1, r_2, \dots) &\approx C(\bar{a}_1, \bar{a}_2, \dots, \bar{r}_1, \bar{r}_2, \dots) \\ &+ \frac{\partial C}{\partial a_1} a'_1 + \frac{\partial C}{\partial a_2} a'_2 + \dots \\ &+ \frac{\partial C}{\partial r_1} r'_1 + \frac{\partial C}{\partial r_2} r'_2 + \dots, \quad (2) \end{aligned}$$

where the overbar indicates the climatological mean and the prime indicates departures from the climatological mean. Since we are interested in cloud variability, we do not concern ourselves with time-mean biases and drop the climatological terms from Eq. (2),

$$C' \approx \frac{\partial C}{\partial a_1} a'_1 + \frac{\partial C}{\partial a_2} a'_2 + \dots + \frac{\partial C}{\partial r_1} r'_1 + \frac{\partial C}{\partial r_2} r'_2 + \dots \quad (3)$$

Another benefit of focusing on departures from climatology is that linearity is more applicable to temporal perturbations of cloud fraction and artifact factors than it is to time-mean relationships.

Corrected cloud fraction anomalies (C^*), which are the component of C influenced by the factors producing real variability (r_i), can be obtained by subtracting the artifact terms from the reported cloud fraction anomaly C' ,

$$C^* \approx C' - \frac{\partial C}{\partial a_1} a'_1 - \frac{\partial C}{\partial a_2} a'_2 - \dots \quad (4)$$

Since values for $\partial C/\partial a_i$ are not known from first principles, we obtain them empirically for each artifact factor via least squares linear regression. Artifact factor anomalies a'_i are the independent variable, cloud fraction anomalies C' are the dependent variable, and $\partial C/\partial a_i$ is the computed regression coefficient. Carrying out linear regression separately for each grid box enables us to take into account that $\partial C/\partial a_i$ varies with different cloud regimes in different grid boxes. We found that higher-order polynomial fits to the $\partial C/\partial a_i$ terms in Eq. (4) did not provide better results than linear regression. We iteratively repeat the above-described procedure several times, since the artifact factors are mostly but not completely linearly independent from each other; almost all spurious variability is removed in the first round. Note that any real variability in cloud fraction that happens to be correlated with variability in artifact factors will be removed by our correction procedure, but we consider a corrected dataset with some real variability removed preferable to a dataset with no real variability removed but dominated by artifacts.

3. Empirical removal of artifacts

a. Original cloud data

Figure 1a shows time series of anomalies in total cloud fraction from ISCCP, PATMOS-x, and *Aqua* MODIS averaged over 60°S–60°N. Variability in the ISCCP and PATMOS-x time series has an obviously different character than that in the MODIS time series. The ISCCP and PATMOS-x time series exhibit much larger changes in cloud fraction than does MODIS, and the

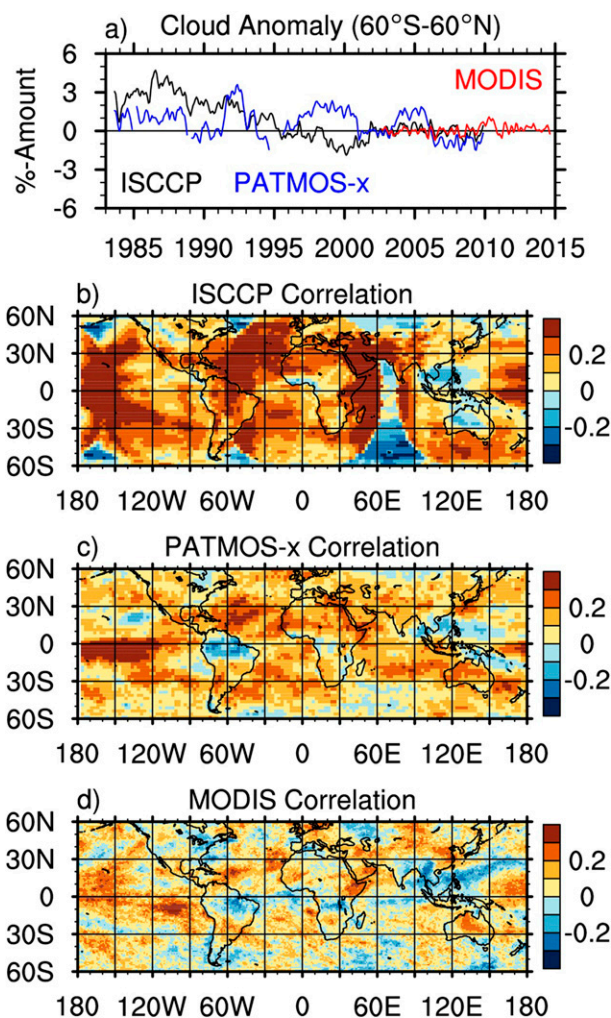


FIG. 1. (a) Daytime-only monthly anomalies in ISCCP (black), PATMOS-x (blue), and *Aqua* MODIS (red) total cloud fraction averaged over all grid boxes between 60°S and 60°N with weighting according to gridbox area. Linear correlation between the time series of daytime-only monthly anomalies in total cloud fraction at each grid box with the time series averaged over 60°S–60°N for (b) ISCCP, (c) PATMOS-x, and (d) *Aqua* MODIS. Anomalies in (a) are referenced from the time period common to all three datasets with 1–2–1 smoothing applied to improve readability.

anomalies in ISCCP and PATMOS-x extend over much longer intervals of time than is the case for MODIS. Figures 1b–d display the correlation between the anomaly time series in each grid box with the time series averaged over 60°S–60°N. An artifact is clearly present in ISCCP, which exhibits unphysical circular patterns of positive correlation corresponding to the areas viewed by geostationary satellites over the United States, Europe, and Japan. In contrast, MODIS shows areas of positive and negative correlation that appear related to natural phenomena, such as the variability of convection in the central tropical Pacific Ocean.

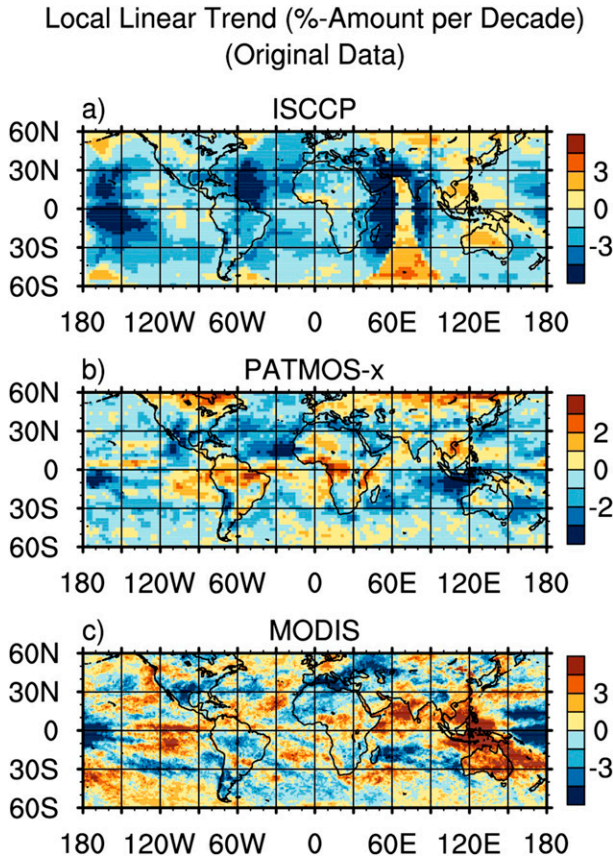


FIG. 2. Local linear trend in daytime-only total cloud fraction monthly anomalies for (a) ISCCP, (b) PATMOS-x, and (c) *Aqua* MODIS. ISCCP and PATMOS-x trends are calculated from July 1983 to December 2009, and MODIS trends are calculated from July 2002 to September 2014.

Figure 2 shows local linear trends in total cloud fraction for ISCCP, PATMOS-x, and *Aqua* MODIS, calculated over the entire record available for each dataset. The spatial pattern of trends in ISCCP cloud fraction is clearly artificial. Locations most frequently viewed by geostationary satellites exhibit decreasing trends and locations most frequently viewed by polar-orbiting satellites exhibit increasing trends. The largest reductions in cloud fraction occur at locations viewed at high satellite zenith angle by three geostationary satellites over the United States, Europe, and Japan. Note that we do not expect the MODIS trend pattern to resemble the ISCCP and PATMOS-x trend patterns because the MODIS time period is shorter and over a different interval than the ISCCP and PATMOS-x time periods.

b. Removal of satellite zenith angle artifact

Satellite retrievals generally report more cloud fraction when the satellite zenith angle is large (Minnis 1989). There are several reasons for this, but one prime

factor is that the pathlength through a cloud layer as viewed from the satellite increases with zenith angle. Specifically, the pathlength is inversely proportional to μ_{sat} , the cosine of the satellite zenith angle. At larger values of $1/\mu_{\text{sat}}$, optically thin and warm clouds are more easily detected than at nadir, and consequently the retrieved cloud fraction increases. Polar-orbiting satellites successively view any particular location on Earth from a variety of zenith angles, but the satellite zenith angle distribution does not vary with location or from month to month and therefore does not produce a systematic artifact in the PATMOS-x or MODIS datasets. The geostationary satellites contributing to ISCCP, however, consistently view different locations with different satellite zenith angles, thus producing systematic spatial biases in certain regions, such as the Indian Ocean sector. Of greater relevance to the present study is that the number and locations of geostationary satellites changed over the ISCCP record, thus altering the satellite zenith angle at many locations. There were three geostationary satellites around Earth in the first part of the ISCCP record and now there are five (see Fig. 2 of Knapp 2008). As more geostationary satellites were added, many locations experienced a systematic decrease in $1/\mu_{\text{sat}}$ and an apparent decrease in cloud fraction (Evan et al. 2007). This is the primary cause of decreasing cloud fraction trends near 30°–60°E, 75°–90°E, 180°–210°E, and 300°–330°E seen in Fig. 2a.

Figure 3a displays the correlation between time series of ISCCP daytime-only total cloud fraction anomalies and μ_{sat} anomalies at each grid box. Since anomalies in μ_{sat} and anomalies in $1/\mu_{\text{sat}}$ exhibit a correlation of -0.95 , we use the former for convenience. Our analysis employs 3-hourly rather than monthly data to capture every possible change occurring in the observing system, but monthly data would produce effectively the same results. Relatively small cloud– μ_{sat} correlation values occur because day-to-day cloud variability is large; at longer time scales, changes in μ_{sat} explain a much larger fraction of cloud variability. As expected, the correlation between cloud anomalies and μ_{sat} anomalies is negative nearly everywhere. Correlation values are largest at locations where the satellite zenith angle is high when only three geostationary satellites view the earth and lower when an additional satellite is available over the United States and over India.

The procedure described in section 2d provides the means of removing spurious variability in cloud fraction associated with changes in satellite zenith angle. We accordingly compute the least squares best-fit line between cloud anomalies and μ_{sat} anomalies. The original cloud anomalies, the μ_{sat} anomalies, and the slope of the best-fit line correspond to the parameters C' , a'_1 , and $\partial C/\partial a_1$ from Eq. (4), respectively. The residuals from the best-fit line

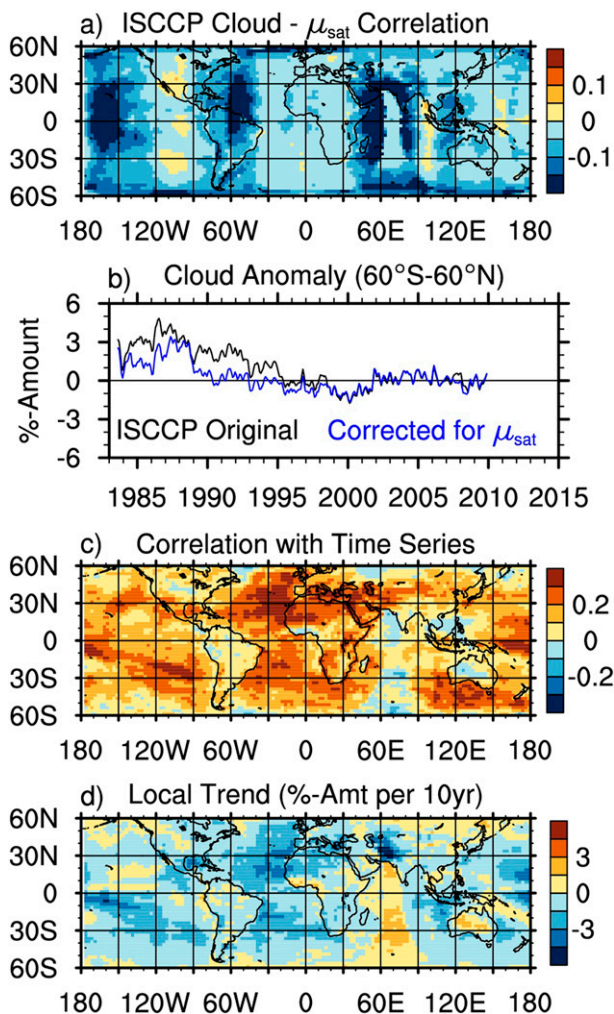


FIG. 3. (a) Linear correlation between the time series of daytime-only 3-hourly anomalies in ISCCP total cloud fraction and cosine of satellite zenith angle (μ_{sat}) at each grid box. (b) As in Fig. 1a, except for ISCCP before (black) and after (blue) removal of spurious variability associated with changes in μ_{sat} . (c) As in Fig. 1b, except for after removal of spurious variability associated with changes in μ_{sat} . (d) As in Fig. 2a, except for after removal of spurious variability associated with changes in μ_{sat} .

become our partly corrected cloud anomalies with minimal artifacts from changes in satellite zenith angle. If no other artifacts were present, the residuals from the best-fit line would correspond to parameter C^* in Eq. (4). We do the calculation separately for each grid box and UTC hour (0000, 0300, 0600, 0900, 1200, 1500, 1800, and 2100), since the impact of satellite zenith angle on cloud fraction retrievals may vary according to the dominant cloud regime and time of day. The time series of corrected cloud anomalies have zero correlation with the time series of μ_{sat} anomalies (not shown).

Figure 3b displays the 60°S–60°N average time series of total cloud fraction anomalies for the original ISCCP

data and for ISCCP data corrected for spurious variability associated with μ_{sat} changes but not other artifacts. Spurious variability due to fluctuations in satellite zenith angle primarily occurs before 1995, when the number and position of geostationary satellites experienced much greater change. A large secular trend is still present in the ISCCP record, albeit of smaller magnitude than in the original data. Figure 3c shows the correlation between the μ_{sat} -corrected anomaly time series in each grid box and the 60°S–60°N time series. Similar to Fig. 1b, unphysical circular patterns of correlation occur in areas viewed by geostationary satellites over the United States, Europe, and Japan. One difference, however, is that larger correlation values no longer exist at locations where satellite zenith angle is high when only three geostationary satellites view the earth (30°–60°E, 75°–90°E, 180°–210°E, and 300°–330°E). Figure 3d displays local linear trends in μ_{sat} -corrected cloud fraction. Circular features still appear, but large trends no longer occur at locations of high satellite zenith angle.

c. Removal of solar zenith angle artifact

The NOAA series of polar-orbiting weather satellites always cross the equator at the same local time of day at the beginning of their missions but drift toward later crossing time as their orbits decay (see Fig. 1 of Heidinger et al. 2014). After several years, the satellites view the earth in the late afternoon rather than the early afternoon. One way this affects cloud retrievals is that a forward model may be less accurate near the terminator. It is also plausible that systematic changes in solar path-length may amplify forward model biases and thereby affect cloud fraction retrievals. Another way a drift toward later crossing time affects cloud retrievals is that a different point in the cloud diurnal cycle is sampled (Foster and Heidinger 2013). If cloud fraction is climatologically greater in late afternoon than early afternoon, a satellite drifting toward a later crossing time will report a spurious increasing trend (i.e., aliasing of the diurnal cycle). Note that the approach of Foster and Heidinger (2013) only explicitly addresses biases caused by aliasing of the diurnal cycle and not problems related to varying solar zenith angle. However, we recognize that the two types of biases (diurnal cycle sampling or other issues stemming from changes in the solar zenith angle) are related, and thus our statistical methods for addressing this bias may produce similar, but not identical, results to those from Foster and Heidinger (2013).

We find that effects from drift through local time can be well approximated by a relationship to the local cosine of solar zenith angle, μ_{sol} . Figure 4a displays the correlation between time series of PATMOS-x daytime-only total cloud fraction anomalies and μ_{sol} anomalies at each grid

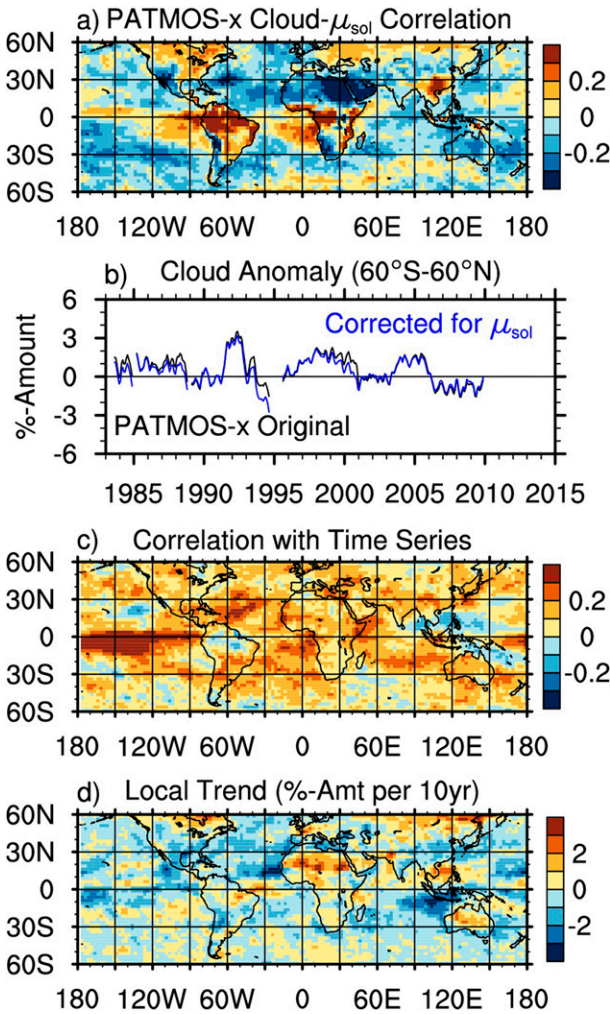


FIG. 4. (a) Linear correlation between the time series of monthly anomalies in PATMOS-x total cloud fraction and cosine of solar zenith angle (μ_{sol}) at each grid box. (b) As in Fig. 1a, except for PATMOS-x before (black) and after (blue) removal of spurious variability associated with changes in μ_{sol} . (c) As in Fig. 1c, except for after removal of spurious variability associated with changes in μ_{sol} . (d) As in Fig. 2b, except for after removal of spurious variability associated with changes in μ_{sol} .

box. Because low-level and high-level clouds have different diurnal cycles and the satellites drifted through only a few hours of local time, it is not straightforward to interpret Fig. 4a in terms of cloud diurnal cycle. Nevertheless, the broad patterns appear physically realistic. Positive correlation values occur over many land areas with convective cloudiness, as would be expected if the cloud fraction is greater in the early afternoon, when the solar zenith angle is smaller and μ_{sol} is larger, than late afternoon, when the solar zenith angle is larger and μ_{sol} is smaller. Negative correlation values occur over most of the ocean, which is consistent with larger total cloud fraction in the late afternoon than the early afternoon.

We remove spurious variability in PATMOS-x total cloud fraction associated with changes in the local time of measurement by computing the least squares best-fit line between cloud anomalies and μ_{sol} anomalies. The original cloud anomalies, the μ_{sol} anomalies, and the slope of the best-fit line correspond to the parameters C' , a'_2 , and $\partial C/\partial a_2$, respectively, from Eq. (4). The residuals from the best-fit line become our partly corrected cloud anomalies with minimal artifacts associated with changes in local solar zenith angle. If no other artifacts were present, then the residuals from the best-fit line would correspond to parameter C^* in Eq. (4). We do the calculation separately for each grid box, since the diurnal cycle of cloudiness varies regionally according to the dominant cloud regime (Cairns 1995). The time series of corrected cloud anomalies have zero correlation with the time series of μ_{sol} anomalies (not shown). We also apply the solar zenith angle correction to ISCCP cloud anomalies, since ISCCP uses polar-orbiting satellite measurements when and where geostationary satellite measurements are not available (mostly poleward of 55° and around 70°E during the earlier part of the record). The correction has a very small impact on the ISCCP dataset due to the overwhelming preponderance of geostationary measurements that regularly provide measurements at the same UTC hours. MODIS cloud data are unaffected by this problem, since the *Aqua* satellite has strictly maintained the same equatorial crossing time.

Figure 4b displays the 60°S–60°N average time series of total cloud fraction anomalies for the original PATMOS-x data and for PATMOS-x data corrected for spurious variability associated with μ_{sol} changes but not other artifacts. Correcting for the local time of measurement makes positive anomalies slightly less positive and negative anomalies slightly less negative. Although removing spurious variability associated with μ_{sol} changes does not have a large impact globally, it is important for certain regions. Figure 4c shows the correlation between the μ_{sol} -corrected anomaly time series in each grid box and the 60°S–60°N time series, and the pattern is changed little from Fig. 1c. Figure 4d displays local linear trends in μ_{sol} -corrected cloud fraction. Trends are more negative over the ocean in Fig. 2b than in Fig. 4d. This is because satellites experienced less drift through local time after the year 2000 and consequently measured cloudiness earlier in the afternoon, on average. Consequently, PATMOS-x reports relatively less cloud fraction over the ocean after 2000 than before 2000, if not corrected. Similarly, PATMOS-x reports relatively more cloud fraction over equatorial Africa and other land regions after 2000 than before 2000, if not corrected.

d. Removal of satellite view area artifact

Figures 3 and 4 indicate that the ISCCP and PATMOS-x records suffer from spurious variability that is unrelated to changes in satellite position and orbital characteristics. For example, a noticeable decrease in PATMOS-x 60°S–60°N average cloud fraction occurs in 1988, 2000, and 2005 when afternoon satellites at the end of their lifetimes are replaced by new ones (Fig. 4b). This likely stems from either intersatellite calibration errors, changes to the channel weighting functions, or a combination of both. PATMOS-x also reported greater cloud fraction for a couple years following the eruption of Mount Pinatubo in 1991 (Fig. 4b), which loaded the lower stratosphere with bright sulfate aerosols and apparently caused more clouds to be identified via a visible reflectance test in the detection algorithm [in ISCCP, the additional reflectivity from Mount Pinatubo aerosols caused thin cirrus clouds to be misidentified as low-level cumulus clouds (Luo et al. 2002)]. Other spurious cloud changes arise from inadvertent mistakes in processing. For example, the use by ISCCP of incorrect calibration coefficients for the *NOAA-18* satellite (Knapp 2008) caused an abrupt increase in reported total cloud fraction at the end of September 2001 (Fig. 3b). Such biases related to calibration, changes in the sensors, errors in ancillary data, or major volcanic eruptions are likely to affect retrieved cloud properties in a similar manner at every location viewed by a satellite.

The rather uniform circular area of positive correlation apparent in Fig. 3c suggests that spatially coherent changes in ISCCP total cloud fraction occur within the area viewed by the European geostationary satellite (see appendix in Norris and Wild 2007), even after removal of spurious variability associated with changes in satellite zenith angle. This supposition is confirmed by Fig. 5a, which displays time series of ISCCP cloud fraction anomalies averaged over northern middle latitudes, southern middle latitudes, and tropical latitudes of the European sector (30°W–30°E). All three latitude zones exhibit a multiyear interval of large positive anomalies during the latter half of the 1980s and similar variations at other times in the record. It is extremely unlikely that any natural process would create similar changes in cloud fraction across such a wide range of latitude. This conclusion is supported by the fact that the correlation between the tropical time series and the northern midlatitude time series is 0.48 for ISCCP and 0.02 for *Aqua* MODIS, both calculated for the 30°W–30°E sector and over their respective time periods. The correlation between the southern midlatitude and tropical time series is 0.39 for ISCCP and 0.01 for MODIS. The fact that the better calibrated MODIS

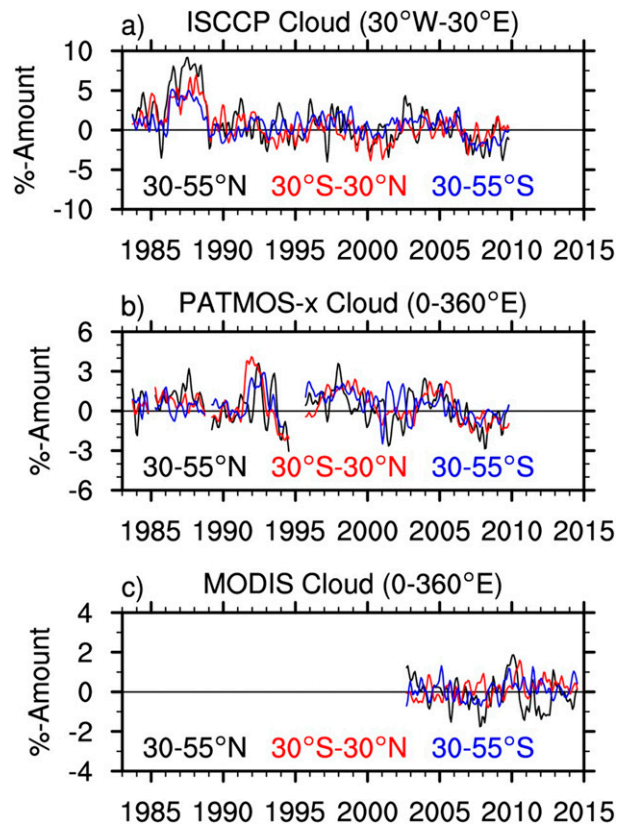


FIG. 5. Daytime-only monthly anomalies in total cloud fraction averaged between 30° and 55°N (black), between 30°S and 30°N (red), and between 30° and 55°S (blue) with weighting according to the gridbox area for ISCCP in the (a) 30°W–30°E sector, (b) PATMOS-x globally, and (c) *Aqua* MODIS globally. Spurious variability related to changes in satellite zenith angle and solar zenith angle was removed from ISCCP and PATMOS-x anomalies prior to plotting. Anomalies are referenced from the time period common to all three datasets with 1–2–1 smoothing applied twice to improve readability.

dataset exhibits near-zero correlation between latitude zones suggests that the substantial ISCCP correlation results from artificial rather than natural causes. Although not shown, coherent variations are also present in northern midlatitude, southern midlatitude, and tropical time series of ISCCP anomalies for other geostationary satellites.

Figure 5b displays time series of PATMOS-x cloud fraction anomalies averaged over northern middle latitudes, southern middle latitudes, and tropical latitudes across all longitudes because a polar-orbiting satellite views the entire globe. All three latitude zones exhibit similar multiyear variations over a large part of the record. The correlation between the tropical time series and the northern midlatitude time series is 0.36 for PATMOS-x but only -0.15 for *Aqua* MODIS, and the correlation between the tropical time series and the

southern midlatitude time series is 0.36 for PATMOS-x but only 0.11 for MODIS. Figure 5c displays time series of *Aqua* MODIS cloud fraction anomalies averaged over northern middle latitudes, southern middle latitudes, and tropical latitudes across all longitudes. Unlike ISCCP and PATMOS-x, MODIS anomalies do not exhibit consistent behavior across all three latitude zones. In the context of spurious variability that is spatially correlated, this is likely because the *Aqua* MODIS-observing system consists of a single instrument that is much better calibrated and has never been replaced.

Although some factors contributing to large-scale spatially coherent artifacts have been identified, many are currently unknown. Moreover, even if a contributing factor is known, it is not necessarily easy to quantify from first principles its impact on retrieved cloud fraction. For this reason, we make the simplifying assumption that artifacts cause the same relative change in total cloud fraction at every location viewed by the satellite. We obtain the presumed artifact anomaly by standardizing anomalies in each grid box separately for each calendar month and then spatially averaging with weighting by grid box area over all grid boxes viewed by a satellite. For PATMOS-x, the spatial average is calculated over 60°S–60°N, since the contributing polar-orbiting satellites viewed the entire globe. For ISCCP, multiple separate spatial averages are calculated over each set of grid boxes to which a particular geostationary or polar-orbiting satellite contributed. Because retrieval methods differ somewhat over ocean, land, and snow/ice-covered surfaces, we calculate separate spatial averages for ocean grid boxes (<50% land), land grid boxes (>50% land), Northern Hemisphere ice/snow grid boxes (>50% ice/snow irrespective of land/ocean), and Southern Hemisphere ice/snow grid boxes. We use two ice/snow categories due to greatly different solar zenith angles in the two hemispheres.

Although some real variability is likely present, we have no means to distinguish it from spurious variability and consequently deem the spatial average standardized anomaly as entirely artificial. The spatial average anomaly is then assigned to each contributing grid box. This builds up an artifact time series for each grid box corresponding to parameter a'_3 from Eq. (4), where each value is the land, ocean, or ice spatial average anomaly for the satellite that viewed the grid box at that time point. For each grid box, we compute the least squares best-fit line between cloud anomalies and artifact anomalies, with the slope of the best-fit line corresponding to parameter $\partial C/\partial a_3$ from Eq. (4). The residuals from the best-fit line become our fully corrected cloud anomalies with minimal spurious variability associated with spatially coherent artifacts. A simple way to view this correction is

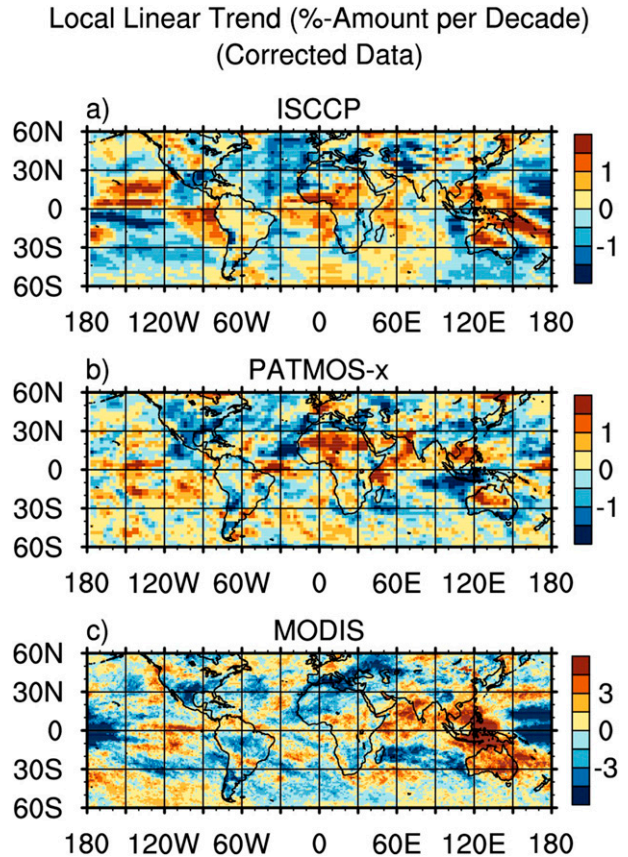


FIG. 6. As in Fig. 2, except for after removal of cloud variability associated with satellite zenith angle changes (ISCCP), solar zenith angle changes (PATMOS-x and ISCCP), and large-scale spatially coherent cloud changes (ISCCP, PATMOS-x, and *Aqua* MODIS).

that we subtract the ocean-mean cloud anomaly from the cloud anomaly in each ocean grid box for each month, subtract the land-mean cloud anomaly from the cloud anomaly in each land grid box for each month, etc. Since the input cloud anomalies have already had variability associated with the μ_{sat} and μ_{sol} anomalies (a'_1 and a'_2) removed and we consider no further artifacts, the residuals from the best-fit line correspond to parameter C^* in Eq. (4). We apply this method to monthly anomalies for PATMOS-x and 3-hourly anomalies for ISCCP, at each UTC hour.

Figure 6a,b display for ISCCP and PATMOS-x, respectively, local linear trends in total cloud fraction after removing variability associated with satellite zenith angle changes, solar zenith angle changes, and large-scale spatially coherent cloud changes. Unlike Fig. 2, the trend patterns appear mostly natural. Between 1983 and 2009, the corrected versions of ISCCP and PATMOS-x both report decreasing cloud fraction over most of the North Atlantic, the Mediterranean region, a large part of the western North Pacific, the ocean around most of

Australia, the ocean south of Mexico, and other locations around the globe. They report increasing cloud fraction over Australia, the South China Sea region, the northwest Indian Ocean, a large part of northern Africa, the eastern subtropical South Pacific, and other locations around the globe. The root-mean-square difference between ISCCP and PATMOS-x grid box trends decreases from 2.0% (the amount per decade for the original data) to 0.9% (the amount per decade for the fully corrected data). Disagreement between ISCCP and PATMOS-x cloud trends may be due to differing satellite instruments and methods of cloud retrieval or remaining artifacts in the datasets. Further validation of the corrected cloud data can be accomplished by comparing variability in cloudiness with variability in physically related meteorological parameters (e.g., Clement et al. 2009).

One critical limitation of our empirically based correction method is that any real variability that is linearly correlated with an artifact factor is removed along with the spurious variability. By removing all cloud variability that is coherent at very large spatial scales, the global average cloud fraction anomaly is constrained by construction to be close to zero. This precludes the use of our corrected ISCCP and PATMOS-x datasets for studies of global mean cloud variability. Despite this shortcoming, the corrected datasets are very useful for investigating regional cloud variability. The local cloud fraction trends displayed in Fig. 6 should be understood as being changes relative to an unknown global mean change. Removing global mean cloud variability has little impact on regional patterns, as illustrated by Fig. 6c, which displays local trends in *Aqua* MODIS total cloud fraction after removing variability associated with large-scale spatially coherent cloud changes. The spatial pattern of trends in Fig. 6c is quite similar to the spatial pattern of trends in Fig. 2c. Note that we do not expect MODIS trends to agree with ISCCP and PATMOS-x trends because they are calculated over different time periods.

e. Further applications

The method described in the previous sections may be employed to remove spurious variability from other ISCCP and PATMOS-x parameters besides total cloud fraction, such as cloud optical thickness, cloud-top height, fraction of particular cloud types, or radiation flux derived from the cloud data. In some cases it may be preferable to transform the variable so that it varies more linearly with radiance, such as performing corrections on the natural logarithm of optical thickness rather than optical thickness. Another concern in applying least squares linear regression is that residuals may not be normally distributed. This is generally not a problem for

total cloud fraction, since it is typically not close to 0% or 100% over the area of an ISCCP or PATMOS-x grid box, but very specific cloud types may have skewed anomaly distributions. For example, ISCCP provides cloud fraction in 42 cloud type categories, defined according to seven cloud-top pressure intervals and six cloud optical thickness intervals. Any single one of these 42 cloud types will have a small climatological value and a frequent occurrence of 0%. To avoid problems associated with the absence of a normal distribution of anomalies, cloud fraction of a single cloud type can instead be obtained by applying the correction procedure to the combined amount of all 42 cloud types, applying the correction procedure to the combined amount of the other 41 cloud types, and then taking the difference to provide the desired cloud type.

Our method removes real variability in cloudiness that is spatially coherent over a large fraction of the area viewed by a satellite. For example, a large fraction of area viewed by the Japanese geostationary satellite is the western tropical Pacific, which experiences substantial changes in cloud fraction associated with the occurrence of El Niño and La Niña. The application of our correction method to the Japanese geostationary satellite view area likely removes some of this real cloud variability, resulting in a weaker cloud response to El Niño/La Niña in the corrected ISCCP dataset than what probably occurs in nature. This outcome can be partially avoided by calculating the best fit between the artifact factor time series and meteorological indices such as the Niño-3.4 SST index and the Southern Oscillation index. The residuals from the best-fit line are artifact factor anomalies that are uncorrelated with the meteorological indices. Use of the revised artifact factor time series in the correction means that the resulting cloud anomaly residuals retain variability linearly related to the meteorological indices. Only meteorological indices that are dominated by subdecadal and higher-frequency variability can be used in this approach; indices such as those for the Pacific decadal oscillation and the Atlantic multidecadal oscillation cannot be used, since their low-frequency variability may project too strongly onto the low-frequency changes of the satellite artifacts.

4. Summary

This study described and applied a method for removing spurious variability in total cloud fraction from two commonly used multidecadal satellite cloud records, ISCCP and PATMOS-x. One cause of spurious variability is systematic changes in the satellite zenith angle of geostationary satellites contributing to the ISCCP dataset. We characterized the effect of change in the satellite zenith angle on reported cloud fraction through linear

regression and obtained corrected cloud anomalies by taking residuals from the best-fit line at each grid box. Another cause of spurious variability is systematic drifts through equatorial crossing time, represented by the solar zenith angle, of polar-orbiting satellites contributing to the PATMOS-x dataset. We characterized the effect of change in the solar zenith angle on reported cloud fraction through linear regression and again obtained corrected cloud anomalies by taking residuals from the best-fit line at each grid box. A third cause of spurious variability are known and unknown changes in effective calibration, ancillary data, and volcanic aerosols that create spatially coherent anomalies in cloud fraction at very large scales in the ISCCP and PATMOS-x datasets. We characterized this effect by creating a time series of normalized cloud anomalies spatially averaged over every grid box viewed by a satellite, calculating the best-fit line between this time series and cloud anomalies at each grid box, and taking residuals to obtain corrected cloud anomalies.

Unlike limited correction procedures for a specific bias (e.g., diurnal cycle in Foster and Heidinger 2013), our approach is general and has been used to correct multiple types of artifacts in more than one cloud dataset. The methods described in this study can be easily applied to additional cloud parameters such as a fraction of individual cloud types, cloud optical thickness, and radiation fluxes derived from the cloud data. One shortcoming of the correction procedure, however, is that any real cloud variability occurring at very large scales is removed along with spurious variability. Consequently, the corrected datasets cannot be used to study global mean cloud changes. Nevertheless, the resulting corrected ISCCP and PATMOS-x datasets are very useful for studying regional changes in clouds arising from natural variability or as a response to global warming. Corrected ISCCP and PATMOS-x data are available from the Research Data Archive at NCAR (Norris and Evan 2015).

Acknowledgments. NOAA Awards NA10OAR4310140 and NA10OAR4310141 supported this work. ISCCP D1 data were obtained from the Atmospheric Science Data Center located at NASA Langley Research Center (https://eosweb.larc.nasa.gov/project/isccp/isccp_table). PATMOS-x data were obtained from the Cooperative Institute for Meteorological Satellite Studies located at the University of Wisconsin–Madison (<http://cimss.ssec.wisc.edu/patmosx/data>). MODIS data were obtained from the NASA Goddard Space Flight Center ordering tool (<http://ladsweb.nascom.nasa.gov/data/search.html>).

REFERENCES

- Baum, B. A., W. P. Menzel, R. A. Frey, D. C. Tobin, R. E. Holz, S. A. Ackerman, A. K. Heidinger, and P. Yang, 2012: MODIS cloud-top property refinements for Collection 6. *J. Appl. Meteor. Climatol.*, **51**, 1145–1163, doi:10.1175/JAMC-D-11-0203.1.
- Cairns, B., 1995: Diurnal variations of cloud from ISCCP data. *Atmos. Res.*, **37**, 133–146, doi:10.1016/0169-8095(94)00074-N.
- Campbell, G. G., 2004: View angle dependence of cloudiness and the trend in ISCCP cloudiness. *13th Conf. on Satellite Meteorology and Oceanography*, Norfolk, VA, Amer. Meteor. Soc., P6.7. [Available online at https://ams.confex.com/ams/13SATMET/techprogram/paper_79041.htm.]
- Clement, A. C., R. Burgman, and J. R. Norris, 2009: Observational and model evidence for positive low-level cloud feedback. *Science*, **325**, 460–464, doi:10.1126/science.1171255.
- Dufresne, J.-L., and S. Bony, 2008: An assessment of the primary sources of spread of global warming estimates from coupled atmosphere–ocean models. *J. Climate*, **21**, 5135–5144, doi:10.1175/2008JCLI2239.1.
- Evan, A. T., A. K. Heidinger, and D. J. Vimont, 2007: Arguments against a physical long-term trend in global ISCCP cloud amounts. *Geophys. Res. Lett.*, **34**, L04701, doi:10.1029/2006GL028083.
- Foster, M. J., and A. Heidinger, 2013: PATMOS-x: Results from a diurnally corrected 30-yr satellite cloud climatology. *J. Climate*, **26**, 414–425, doi:10.1175/JCLI-D-11-00666.1.
- Free, M., and B. Sun, 2013: Time-varying biases in U.S. total cloud cover data. *J. Atmos. Oceanic Technol.*, **30**, 2838–2849, doi:10.1175/JTECH-D-13-00026.1.
- Heidinger, A. K., A. T. Evan, M. J. Foster, and A. Walther, 2012: A naive Bayesian cloud detection scheme derived from CALIPSO and applied to PATMOS-x. *J. Appl. Meteor. Climatol.*, **51**, 1129–1144, doi:10.1175/JAMC-D-11-02.1.
- , M. J. Foster, A. Walther, and X. Zhao, 2014: The Pathfinder Atmospheres–Extended (PATMOS-x) AVHRR climate dataset. *Bull. Amer. Meteor. Soc.*, **95**, 909–922, doi:10.1175/BAMS-D-12-00246.1.
- Jacobowitz, H., L. L. Stowe, G. Ohring, A. K. Heidinger, K. Knapp, and N. R. Nalli, 2003: The Advanced Very High Resolution Radiometer Pathfinder Atmosphere (PATMOS) climate dataset: A resource for climate research. *Bull. Amer. Meteor. Soc.*, **84**, 785–793, doi:10.1175/BAMS-84-6-785.
- Klein, S. A., Y. Zhang, M. D. Zelinka, R. Pincus, J. Boyle, and P. J. Gleckler, 2013: Are climate model simulations of clouds improving? An evaluation using the ISCCP simulator. *J. Geophys. Res. Atmos.*, **118**, 1329–1342, doi:10.1002/jgrd.50141.
- Knapp, K., 2008: Calibration assessment of ISCCP geostationary infrared observations using HIRS. *J. Atmos. Oceanic Technol.*, **25**, 183–195, doi:10.1175/2007JTECHA910.1.
- Luo, Z., W. B. Rossow, T. Inoue, and C. J. Stubenrauch, 2002: Did the eruption of Mt. Pinatubo volcano affect cirrus properties? *J. Climate*, **15**, 2806–2820, doi:10.1175/1520-0442(2002)015<2806:DTEOTM>2.0.CO;2.
- Minnis, P., 1989: Viewing zenith angle dependence of cloudiness determined from coincident GOES East and GOES West data. *J. Geophys. Res.*, **94**, 2303–2320, doi:10.1029/JD094iD02p02303.
- Norris, J. R., 1999: On trends and possible artifacts in global ocean cloud cover between 1952 and 1995. *J. Climate*, **12**, 1864–1870, doi:10.1175/1520-0442(1999)012<1864:OTAPAI>2.0.CO;2.
- , 2000: What can cloud observations tell us about climate variability. *Space Sci. Rev.*, **94**, 375–380, doi:10.1023/A:1026704314326.
- , and M. Wild, 2007: Trends in aerosol radiative effects over Europe inferred from observed cloud cover, solar “dimming,” and solar “brightening.” *J. Geophys. Res.*, **112**, D08214, doi:10.1029/2006JD007794.

- , and A. Slingo, 2009: Trends in observed cloudiness and Earth's radiation budget: What do we not know and what do we need to know? *Clouds in the Perturbed Climate System: Their Relationship to Energy Balance, Atmospheric Dynamics, and Precipitation*, J. Heintzenberg and R. J. Charlson, Eds., Strüngmann Forum Reports, MIT Press, 17–36.
- , and A. T. Evan, 2015: Cloud properties from ISCCP and PATMOS-x corrected for spurious variability related to changes in satellite orbits, instrument calibrations, and other factors. Research Data Archive, Computational and Information Systems Laboratory, NCAR, Boulder, CO, doi:10.5065/D62J68XR.
- Ramanathan, V., R. D. Cess, E. F. Harrison, P. Minnis, B. R. Barkstrom, E. Ahmad, and D. Hartmann, 1989: Cloud-radiative forcing and climate: Results from the Earth Radiation Budget Experiment. *Science*, **243**, 57–63, doi:10.1126/science.243.4887.57.
- Rosow, W. B., and R. A. Schiffer, 1999: Advances in understanding clouds from ISCCP. *Bull. Amer. Meteor. Soc.*, **80**, 2261–2287, doi:10.1175/1520-0477(1999)080<2261:AIUCFI>2.0.CO;2.
- , A. W. Walker, D. E. Beuschel, and M. D. Roiter, 1996: International Satellite Cloud Climatology Project (ISCCP): Documentation of new cloud datasets. WMO Tech. Doc. WMO/TD-737, 115 pp. [Available online at <http://isccp.giss.nasa.gov/pub/documents/d-doc.pdf>.]
- Stocker, T. F., and Coauthors, 2013: *Climate Change 2013: The Physical Science Basis*. Cambridge University Press, 1535 pp. [Available online at www.climatechange2013.org/images/report/WG1AR5_ALL_FINAL.pdf.]